Periodically Switched Nonlinear Structures for Frequency Conversion: Theory and Experimental Demonstration

David Artigas, Edik U. Rafailov, *Member, IEEE*, Pablo Loza-Alvarez, and Wilson Sibbett

***Abstract*—In this paper, we report on the analytical study of a first-order quasi-phase-matched structure based on a periodically switched nonlinearity. The general average equations describing parametric wave interaction for this structure are obtained. The theoretical results are then used to analyze the special case of a device based on a semiconductor $Al_xGa_{1-x}As$ waveguide for efficient frequency doubling in the mid-infrared to the far-infrared range. The necessary conditions to obtain an optimal configuration are discussed in both continuous wave and femtosecond-pulse regimes. Our analysis indicates that the conversion efficiency obtained should significantly exceed the efficiency obtained with a periodically poled lithium niobate crystal at long wavelengths. Finally, we include the preliminary results of the experimental demonstration of a waveguide device based on alternating domains of GaAs and $Al_{0.4}Ga_{0.6}As$.**

***Index Terms*—Nonlinear optics, parametric devices, quasi-phase matching, second-harmonic generation, ultrafast optics.**

I. Introduction

THERE is an increasing interest for obtaining compact tunable optical sources for the near-infrared and, more particularly, for mid-infrared wavelength ranges. Successful implementation of compact sources in these spectral regions can be expected to make a positive impact on a variety of applications, such as remote sensing, atmospheric transmission, and photomedicine. The devices that are used at present are typically based on narrow-bandgap semiconductor lasers and quantum cascade lasers. However, these are restricted to low CW or average pulsed output power levels at room temperature or may require cooling to liquid nitrogen temperature. Additionally, they also have limited ($<$140 nm) tunability. Frequency conversion must therefore regarded as a practical alternative.

Progress in the development of electric-field poling techniques for the patterning of the domain structure of ferroelectric crystals has enabled the implementation of quasi-phase-matched (QPM) structures for efficient frequency conversion interactions [1]. By employing this technique, it is possible to exploit, within the transparency range of the material, the largest available nonlinear coefficient. Such QPM devices have been fabricated using ferroelectric materials [2]–[4] and involving a wide variety of device structures [5]. There is also a major interest in fabricating semiconductor-based QPM structures because they offer several advantages over the conventional ferroelectric-based QPM counterparts. Notable advantages include larger nonlinear coefficients ($\sim$170 pm/V) [6], higher optical damage thresholds, and a larger transparency range with low absorption. Several attempts to fabricate semiconductor QPM devices in bulk [7]–[10] or waveguide [11]–[20] configurations have been explored already. These include the stacking of thin plates for first-order QPM [7], [8], epitaxial growth for orientation-patterned GaAs films [9], [10], [21], [22], quantum-well intermixing induced by ion implantation [13]–[16], and periodic domain inversion by wafer bonding [17] and by regrowth techniques [19]. Analogously, several studies for optimizing the conversion efficiency in semiconductor waveguides have been reported [23], [24] and a number of candidates, such as AlGaAs [18], InSb [25], and GaN [26], have been identified for frequency up/down conversion, such that the operation range can be extended from the far-infrared to the visible.

In this paper, we describe a technique that involves a periodical switching of the nonlinear coefficient [periodically switched nonlinearity (PSN)] to produce a first-order QPM for frequency mixing applications. This technique applies to any material within its transparency range and can be used to exploit the largest available nonlinear coefficient in those cases where periodically poled QPM is not possible. We have undertaken a theoretical analysis of this structure, including the deduction of the governing averaged equations of the device and the required phase-matching conditions for efficient frequency conversion. A theoretical comparison of the special case of a semiconductor $Al_xGa_{1-x}As$ waveguide PSN with bulk periodically poled lithium niobate (PPLN) has been performed and this has shown a higher efficiency for the PSN structure in the mid-to-far-infrared range. The preliminary demonstration of the technique in a GaAs–AlGaAs waveguide structure is also reported.

II. Periodically Switched Nonlinearity

A simplified scheme of a PSN device is illustrated in Fig. 1. For the PSN effect to occur, the nonlinear optical coefficient in

Manuscript received October 20, 2003; revised April 6, 2004. The work of P. Loza-Alvarez was supported by the European Regional Development Fund and the Ministerio de Ciencia y Tecnología through the Ramón y Cajal program. This work was supported in part by the Generalitat de Catalunya, the Spanish Government under Grant TIC2000-1010, and the Engineering and Physical Sciences Research Council (EPSRC).

D. Artigas and P. Loza-Alvarez are with the ICFO-Institut de Ciències Fotòniques and the Department of Signal Theory and Communications, Universitat Politècnica de Catalunya, 08034 Barcelona, Spain (e-mail: david@tsc.upc.es).

E. U. Rafailov and W. Sibbett are with the School of Physics and Astronomy, University of St. Andrews, North Haugh, St. Andrews, Fife KY16 9SS, U.K.

Digital Object Identifier 10.1109/JQE.2004.831644

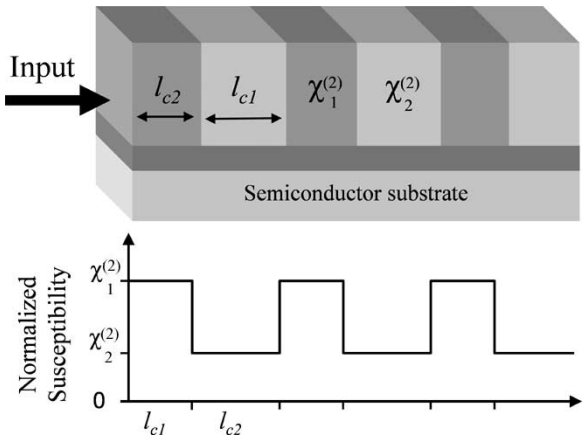

Fig. 1. Simplified scheme of a periodically switched nonlinearity in a GaAs and AlGaAs device.

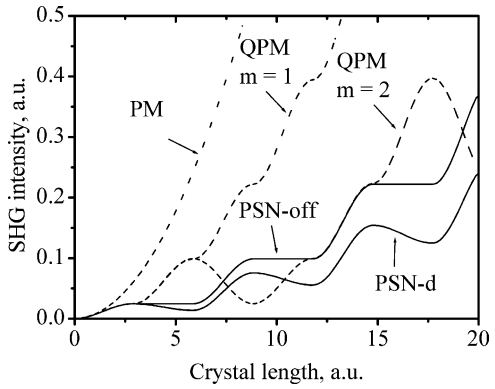

Fig. 2. Comparison of SHG output powers for different QPM designs. The labels indicate the different phase-matching techniques. PM: birrefringent phase-matching; QPM $-$ m $=$ 1: first-order periodically polled QPM; QPM $-$ m $=$ 2: second-order periodically polled QPM with duty cycle $D = 1/4$; PSN-d: decreased PSN; PSN-off: switch-off PSN.

the material $\chi_1^{(2)}$ has to be decreased to $\chi_2^{(2)}$ or even switched off $(\chi_2^{(2)} = 0)$ periodically to form, respectively, the so-called PSN-d or PSN-off structures. In practice, there are several methods that can be used to produce these PSN devices. One approach to reducing or canceling the effective nonlinear coefficient of the material is based on ion implantation (e.g., high-energy helium ions) and intermixing techniques. It has been demonstrated that such a technique can effectively switch off the nonlinearity in the implanted zone in both $LiNbO_3$-based crystals [27] and in semiconductors [28]. This technique was used to demonstrate PSN structures in ZnSe [29]. Importantly, in the case of quantum-well (QW) intermixing in semiconductors [30], it has been shown that ion implantation does not introduce significant optical losses [31]. Another technique to achieve PSN devices is based on a regrowth process. By regrowth, it is possible to replace the original material with one that exhibits a smaller nonlinear coefficient (see Fig. 1). In particular, it has been shown that there is a reduction in the magnitude of the susceptibility coefficient $\chi^{(2)}$ for an increasing Al content in the $Al_xGa_{1-x}As$ system, which is consistent with Miller's rule [32]. Based on his concept, a PSN device was implemented initially to obtain second-harmonic generation (SHG) using a reflection geometry [33]. Interestingly, all of these methods can be readily implemented such that provision for this switching of the nonlinearity can be selected to be periodic along the propagation axis of the crystals. This periodicity in the device structure can be designed to satisfy quasi-phase-matching conditions in first-order or higher order QPM structures. As discussed in Section III, the optimal design is obtained when the length of each domain is equal to the respective coherent length.

In Fig. 2, the expected behavior of the SHG output power is calculated for different QPM designs. As this figure shows, the SHG efficiency for the PSN structures design is less efficient than that for a first-order QPM scheme. However, PSN structures offer an important advantage: they can be implemented in situations where periodically poled schemes are extremely difficult or impossible to implement. For example, this technique can be applied for efficient generation in the blue/ultraviolet (UV) range using available electronic beam lithography in crystals such as potassium titanyl phosphate [$KTiOPO_4$ (KTP)]. In other materials such as polymers, by stacking thin films of two adequate materials, the technique could provide an additional advantage whereby large spatial walk-off within the material could be compensated. Also, with the use of an ion implantation technique, it is possible to fabricate channel waveguides [34] and PSN gratings simultaneously such that the optical power density can be increased inside the material to provide a greater compatibility with lower power diode lasers [35]. Additionally, the PSN-d structures can be implemented in $Al_xGa_{1-x}As$ wafers to form first-order QPM devices for which the grating periods are restricted in length only by the limit imposed by the etching and electronic beam lithography technologies (>200 nm).

III. Model

A. Theoretical Analysis

To assess the potential of PSN structures, a detailed theoretical and numerical analysis was undertaken. The model employed was based on the slowly varying envelope approximation (SVEA) which describes pulse evolution in a collinear SHG configuration [36]. The model includes group-velocity mismatch (GVM), second-order group-velocity dispersion (GVD), and periodic second-order nonlinearity. The coupled-wave equations describing the propagation inside one domain are

$$i\frac{\partial A_{Fq}(z,t)}{\partial z} + ik'_{Fq}\frac{\partial A_{Fq}(z,t)}{\partial t} - \frac{1}{2}k''_{Fq}\frac{\partial^2 A_{Fq}(z,t)}{\partial t^2} + \Gamma_{Fq}A^*_{Fq}(z,t)A_{Hq}(z,t)\exp(i\Delta k_q z) = 0 \quad (1)$$

$$i\frac{\partial A_{Hq}(z,t)}{\partial z} + ik'_{Hq}\frac{\partial A_{Hq}(z,t)}{\partial t} - \frac{1}{2}k''_{Hq}\frac{\partial^2 A_{Hq}(z,t)}{\partial t^2} + \Gamma_{Hq}A^2_{Fq}(z,t)\exp(-i\Delta k_q z) = 0 \quad (2)$$

where $A_{iq}(z,t)$ is the slowly varying complex amplitude. The subscript refers to the fundamental $(i = F)$ and SH $(i = H)$ waves, as well as the material properties at the first $(q = 1)$ and second $(q = 2)$ domains. The nonlinear coefficient in each domain d_q is included within (1) and (2) by way of the parameters $\Gamma_{Fq} = 2\omega_F d_q/n_{Fq}c$ and $\Gamma_{Hq} = \omega_H d_q/n_{Hq}c$. The wave number is defined as $k_{iq} = (2\pi/\lambda_i)n_{iq}(\lambda_i)$ where the primes indicate the derivative with respect to angular frequency

ω_i. The refractive indices n_{iq} were calculated using the Sellmeier equations in [37]. Finally, the wavevector mismatch is $\Delta k_q = k_{Hq} - 2k_{Fq}$.

We took into account the boundary condition for the field at the interfaces between the different PSN domains by introducing the Fresnel transmission coefficients as follows:

$$\tau_{i1} = \frac{2k_{i1}}{k_{i1}+k_{i2}}$$
$$\tau_{i2} = \frac{2k_{i2}}{k_{i1}+k_{i2}}. \tag{3}$$

The generation of backward waves propagating in the negative z direction is not considered because the grating period is much longer than the optical period and Bragg reflection can be neglected. It should also be noted that (1) and (2) can be extended to the more general case of three-wave-mixing interaction such as optical parametric oscillation (OPO) and sum/difference frequency mixing (S/DFM). Fig. 2 were obtained by directly solving (1) and (2) in the CW regime.

All of the coefficients defining the PSN structure in (1) and (2), i.e., n_{iq}, k'_{iq}, k''_{iq}, Δk_q, and d_q, change periodically according to the length of each domain l_q, with a period $\Lambda = l_1 + l_2$. Therefore, in order to compare the performance of the PSN structure with other materials, it is convenient to obtain a set of averaged equations. By performing a Fourier expansion of all the fields and parameters, it is possible to define the averaged nonlinear coefficient, phase-mismatch, GVM, and GVD. For convenience, we first redefine the field amplitude as

$$a_{iq} = \sqrt{n_{iq}} A_{iq}. \tag{4}$$

Thus, the pulse energy can be written as

$$J = \varepsilon_0 c/2 \int_{-\infty}^{\infty} \left[|a_{Fq}|^2 + |a_{Hq}|^2\right] dt. \tag{5}$$

The scaling [see (4)] yields averaged equations which exhibit a conservative quantity directly related to the actual averaged energy, as shown below. Additionally, using this scaling, the resulting nonlinear parameters $\Gamma_{Fq} = 2\omega_F\sqrt{f_q}/c$ and $\Gamma_{Hq} = \omega_H\sqrt{f_q}/c$ include the familiar figure of merit (FOM) for SHG $f_q = d_q^2/(n_{Fq}^2 n_{Hq})$. We then expand the amplitude envelope and all the periodic functions in Fourier series as

$$a_{iq} = \sum_n b_{in} \exp[in\kappa z] \tag{6}$$
$$k'_{iq} = \sum_n K'_{in} \exp[in\kappa z]$$
$$k''_{iq} = \sum_n K''_{in} \exp[in\kappa z] \tag{7}$$

and

$$\begin{cases} \sqrt{f_q}\exp[i\Delta k_q z] = \frac{d_q}{n_{Fq}\sqrt{n_{Hq}}}\exp[i\Delta k_q z] \\ \qquad\qquad = \sum_n D_{Fn}\exp[i(n\kappa + \overline{\Delta k})z] \\ \sqrt{f_q}\exp[-i\Delta k_q z] = \frac{d_q}{n_{Fq}\sqrt{n_{Hq}}}\exp[-i\Delta k_q z] \\ \qquad\qquad = \sum_n D_{Hn}\exp[i(n\kappa - \overline{\Delta k})z] \end{cases} \tag{8}$$

where $\kappa = 2\pi/\Lambda$. The phase mismatch in (1) and (2) can be divided into two terms, namely $\Delta k_q z = \overline{\Delta k} z + g(z)$. The first term, $\overline{\Delta k} = (\Delta k_1 l_1 + \Delta k_2 l_2)/\Lambda$, is an averaged phase matching, and the second term $g(z)$, defined as follows:

$$g(z) = \begin{cases} (\Delta k_1 - \overline{\Delta k})z, & 0 \le z < l_1 \\ (\Delta k_2 - \overline{\Delta k})z, & -l_2 \le z < 0 \end{cases} \tag{9}$$

retains the periodic variation in the phase, modifying the Fourier coefficient D_{in}. Finally, we introduce losses in (1) and (2), including interface Fresnel reflections together with the linear absorption in the material (γ_i) as

$$\alpha_i = -\frac{1}{\Lambda}\ln(\tau_{i1}\tau_{i2}) + \gamma_i. \tag{10}$$

Introducing (4), (6)–(8), and (10) in (1) and (2) and retaining only the lowest order terms (higher order Fourier components introduce averaged third-order nonlinearities [38]–[40], but are negligible under the conditions studied here), we obtain the averaged equations for the dc components b_{10} and b_{20} as follows:

$$i\frac{\partial b_{F0}(z,t)}{\partial z} + iK'_{F0}\frac{\partial b_{F0}(z,t)}{\partial t} - \frac{1}{2}K''_{F0}\frac{\partial^2 b_{F0}(z,t)}{\partial t^2} + i\alpha_F b_{F0} + \frac{2\omega_F}{c}D_{F,-1}b^*_{F0}(z,t)b_{H0}(z,t)e^{i\varepsilon z} = 0 \tag{11}$$

$$i\frac{\partial b_{H0}(z,t)}{\partial z} + iK'_{H0}\frac{\partial b_{H0}(z,t)}{\partial t} - \frac{1}{2}K''_{H0}\frac{\partial^2 b_{H0}(z,t)}{\partial t^2} + i\alpha_H b_{H0} + \frac{\omega_H}{c}D_{H,1}b^2_{F0}(z,t)e^{-i\varepsilon z} = 0 \tag{12}$$

where the residual phase mismatch is defined as $\varepsilon = \overline{\Delta k} - \kappa$. These averaged equations are formally equal to (1) and (2). Therefore, the averaged dispersion parameters and nonlinear coefficients in (11) and (12), which correspond to the Fourier coefficients of the expansion series, are the key parameters of this problem, retaining its main physics. Then we can define an averaged GVM

$$\delta = K'_{H0} - K'_{F0} \tag{13}$$

with

$$K'_{i0} = \frac{(k'_{i1}l_1 + k'_{i2}l_2)}{\Lambda} \tag{14}$$

and an averaged GVD as

$$K''_{i0} = \frac{(k''_{i1}l_1 + k''_{i2}l_2)}{\Lambda}. \tag{15}$$

Note that in structures like these we gain, as (14) and (15) show, a new degree of freedom to engineer the dispersion coefficient. The averaged nonlinear coefficients are

$$D_{F,-1} = \frac{d_1}{in_{F1}\sqrt{n_{H1}}}\frac{(\exp[i(\Delta k_1 - \varepsilon)l_1] - 1)}{(\Delta k_1 - \varepsilon)\Lambda} - \frac{d_2}{in_{F2}\sqrt{n_{H2}}}\frac{(\exp[-i(\Delta k_2 - \varepsilon)l_2] - 1)}{(\Delta k_2 - \varepsilon)\Lambda} \tag{16}$$

$$D_{H,1} = -\frac{d_1}{in_{F1}\sqrt{n_{H1}}}\frac{(\exp[-i(\Delta k_1 - \varepsilon)l_1] - 1)}{(\Delta k_1 - \varepsilon)\Lambda} + \frac{d_2}{in_{F2}\sqrt{n_{H2}}}\frac{(\exp[i(\Delta k_2 - \varepsilon)l_2] - 1)}{(\Delta k_2 - \varepsilon)\Lambda}. \tag{17}$$

Equations (16) and (17) fulfill $D_{H,1} = D^*_{F,-1}$, allowing the definition of a conserved magnitude as the averaged energy in the form

$$J_0 = \frac{\varepsilon_0 c}{2} \int_{-\infty}^{\infty} \left[|b_{F0}|^2 + |b_{H0}|^2 \right] dt. \tag{18}$$

In addition, $|D_{H,1}|^2$ defines the nonlinear FOM for SHG in PSN.

The present theoretical development constitutes a generalization of a similar analysis, previously performed for a simplified structure [39], [40]. Here we have considered the situation in which the structure has two domains with different lengths ($l_1 \neq l_2$). This has two consequences in the theoretical development. First, an averaged phase mismatch cannot be defined *a priori*, since the modification of the nonlinear coefficient caused by $g(z)$ would not be considered. Second, by including the refractive index in the nonlinear term, the resulting average equations do not require higher order terms. In addition, as an averaged refractive index is no longer defined, the redefinition of the field amplitude in (4) allows to obtain an average energy in the form of (18), which is consistent with the averaged equations (16) and (17).

B. Phase-Matching Condition

Phase matching occurs when the residual phase mismatch is $\varepsilon = 0$, resulting in $\Delta k_1 l_1 + \Delta k_2 l_2 = 2\pi$. Here, the pair of values l_1 and l_2 affect the averaged nonlinear coefficient (16) and (17), thus the role of l_1 and l_2 in these equations is similar to the duty cycle error in periodically poled ferroelectric crystals. As a consequence, the domain lengths l_1 and l_2 must be chosen to maximize the averaged nonlinear coefficient. By making the length of the two domains equal to their respective coherent length, i.e., $l_1 = l_{c1}$ and $l_2 = l_{c2}$, with

$$\begin{aligned} l_{c1} &= \frac{\pi}{\Delta k_1} \\ l_{c2} &= \frac{\pi}{\Delta k_2} \end{aligned} \tag{19}$$

the conditions $\varepsilon = 0$ and $\Delta k_q l_{cq} = \pi$ are fulfilled, obtaining the maximum averaged nonlinear coefficient as follows:

$$D_{H,1} = \frac{2}{i\pi} \left(\frac{d_1}{n_{F1}\sqrt{n_{H1}}} \frac{l_{c1}}{\Lambda} - \frac{d_2}{n_{F2}\sqrt{n_{H2}}} \frac{l_{c2}}{\Lambda} \right) = D^*_{F,-1}. \tag{20}$$

It is important to note that the coherence lengths are generally different in each domain.

As an example, Fig. 3(a) and (b) shows the results for a QPM situation and a phase-mismatched situation, respectively for both the direct solution of (1) and (2) and the averaged solution given by (11) and (12) in the femtosecond-pulse regime. As the figure shows, the process is efficient when SHG in the first domain is higher than back conversion in the second one.

Equation (20) can be used as an initial design condition. First, note that, when $d_2 = -d_1$, $n_{i1} = n_{i2}$, and $l_{c1} = l_{c2}$, (20) reduces to the square root of the FOM for the effective nonlinear coefficient in periodically poled QPM, i.e., $\sqrt{f_{pp}} = 2d_{\text{eff}}/(\pi n_F \sqrt{n_H})$. This result shows that periodically poling is the optimal situation and should be used when possible. In those cases where it is not possible, the best alternative is the PSN-off configuration, in which $d_2 = 0$. Here the effective nonlinear coefficient is half of that obtained when using periodic poling and is equivalent to a second-order QPM structure (as shown in Fig. 2). Less efficient is the case of PSN-d in which the two different materials in each domain have a positive value of d_q. Here, in order to have an effective nonlinear coefficient, both terms in (20) must be different. This can be achieved by using two materials with a large difference in their nonlinear coefficients d_1 and d_2 (referred to as case A in Section III-C) and/or by choosing two media with different dispersive properties, resulting in a large difference in the dispersion factor $l_{cq}/(n_{Fq}\sqrt{n_{Hq}})$ (case B).

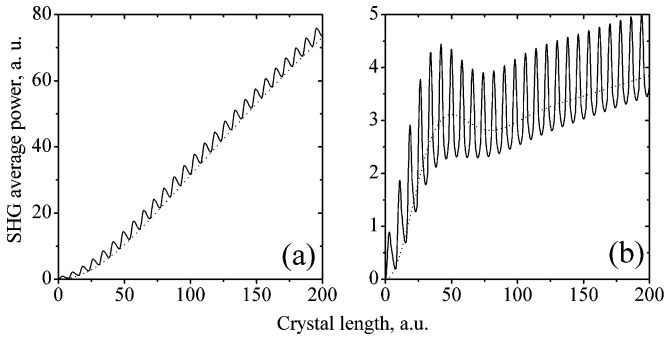

Fig. 3. SHG average power for 100-fs pump pulses in GaAs–$Al_{0.4}Ga_{0.6}As$ PSN structures. The solid lines correspond to the direct solution of (1) and (2) and the dashed lines to the solution of the averaged equations (11) and (12) for (a) a QPM situation ($l_1 = l_c = 2.97\ \mu$m and $l_2 = l_d = 4.73\ \mu$m) and (b) a phase-mismatch case ($l_1 = l_2 = 4\ \mu$m).

C. An Interesting Case: $Al_xGa_{1-x}As$

In this section, we explore numerically the performance of PSN structures. Due to the interest of applying this technique for its use in semiconductors materials [19], [25], [33], we decided to investigate a PSN structure formed by grown layers of $Al_xGa_{1-x}As$ (PSN-d) and by ion implantation on GaAs (PSN-off). The results are then compared with a conventional bulk PPLN crystal, given that this material is becoming standard for wavelength conversion applications. For analysis purposes, we used the nonlinear coefficients d_{14} for $Al_xGa_{1-x}As$ in [28] (170 pm/V for GaAs, $d_{14} = 130$ pm/V for $Al_{0.42}Ga_{0.58}As$ and $d_{14} = 39$ pm/V for AlAs) and $d_{33} = 27$ pm/V for PPLN. Miller's Δ was used for wavelength scaling the nonlinear coefficients to provide consistence with recent measurements of the GaAs nonlinear coefficient at 4 μm [9]. The Sellmeier equations for $Al_xGa_{1-x}As$ in [37] and $LiNbO_3$ in [41] were used.

To choose the best PSN-d configuration, reference is made to Fig. 4(a) where we show the FOM ($|D_{H1}|^2$) in terms of the mole fraction of aluminum x at a fundamental wavelength of 2 μm. As can be expected, the plot is symmetric with respect to the diagonal (bulk material). A different situation where $|D_{H1}|^2 = 0$ is shown by the dashed line. This situation occurs when the two terms in (20) are equal and divides the plot into two regions, cases A and B, as mentioned previously. Notice that the maximum in region A, corresponding to $Al_{0.4}Ga_{0.6}As$–AlAs, is due to the much larger value of d_{14} in $Al_{0.4}Ga_{0.6}As$. In contrast, the maximum in region B, corresponding to $Al_{0.4}Ga_{0.6}As$–GaAs, is due to the large value of $l_{cq}/(n_{Fq}\sqrt{n_{Hq}})$ for $Al_{0.4}Ga_{0.6}As$

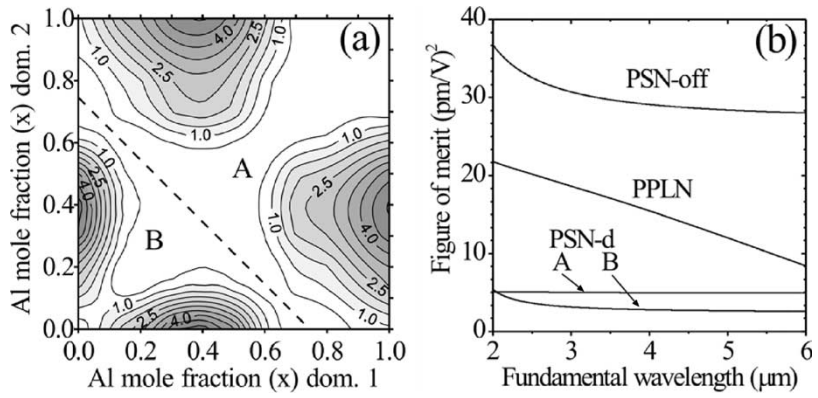

Fig. 4. (a) SHG FOM for PSN-d structures based on $Al_xGa_{1-x}As$ in terms on the mole fraction of aluminum. (b) FOM for PPLN, GaAs switch-off PSN, $Al_{0.4}Ga_{0.6}As$–AlAs (case A) and $Al_{0.4}Ga_{0.6}As$–GaAs (case B) PSN-d in terms of the pump wavelength. As a reference, the FOM of a periodically poled GaAs crystal would be twice that of the PSN-off.

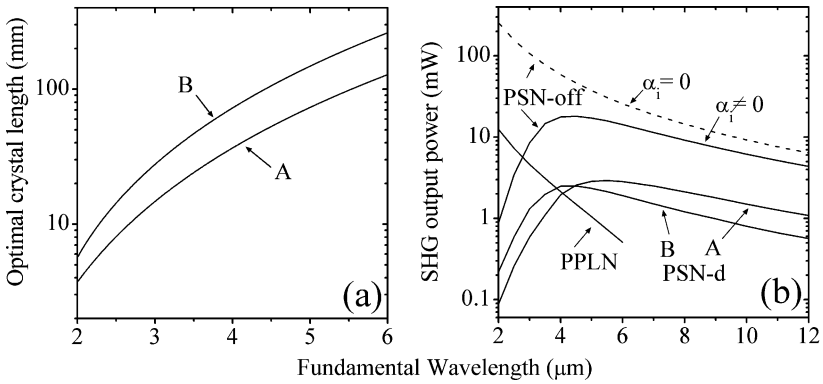

Fig. 5. (a) Optimal crystal length L_α in $Al_{0.4}Ga_{0.6}As$–AlAs (case A) and $Al_{0.4}Ga_{0.6}As$–GaAs (case B) PSN-d structures. (b) Calculated CW SHG output power versus pump wavelength. PSN structures lengths are given by L_α but limited to $L = 30$ mm in order to compare with PPLN (crystal length fixed to $L = 30$ mm.). The dashed line shows conversion for a switch-off PSN structure assuming no reflection losses. The averaged pump power is 1 W.

rather than the particular value of d_{14} in each domain. In the subject matter that follows, the performances of these two optimal PSN-d configurations (cases A and B), together with PSN-off devices, are compared and contrasted with the performances of bulk PPLN crystals. In Fig. 4(b), we plot the FOM for all these cases in the range of transparency of the PPLN crystal. From this figure, we see that the highest value of the FOM corresponds to the PSN-off structure. This is due to the large nonlinear coefficient d_{14} of GaAs when compared to the d_{33} coefficient of PPLN. Also note that, in case A of PSN-d, the FOM remains constant with the wavelength. This is because the evolution of the dispersion term $l_{cq}/(n_{Fq}\sqrt{n_{Hq}})$ compensates for the decrease of the nonlinear coefficient d_{14}. This shows the possibility of increasing the efficiency of a PSN device by engineering the dispersion.

The analysis described above implies some advantages of PSN devices. However, two effects limit its efficiency. The first is the reflection losses due to the high difference in the refractive index between domains. This results in a limit in the maximum length of our PSN-d device and is especially important in the CW regime. The second one is the large average GVM present in semiconductor materials, which is especially important in the femtosecond-pulse regime.

In the CW case, the FOMs shown in Fig. 4(b) could lead to the conclusion that PSN-off structures always offer the best conversion efficiency. This, however, is not always the case. From the practical point of view, reflection losses result in an optimal crystal length L_α at which there is a maximum conversion efficiency. An approximate expression for L_α can be found by solving (11) and (12) in the CW regime, within the nondepletion approximation $(D_{F,-1} = 0)$. The solution for these equations is

$$b_{H0} = i\frac{\omega}{c}D_{H,1}\left(\frac{\exp[-\alpha_H z] - \exp[-2\alpha_F z]}{2\alpha_F - \alpha_H}\right)b_{F0}^2. \quad (21)$$

By maximizing this expression, one obtains the optimal crystal length as

$$L_\alpha = \frac{\ln(2\alpha_F/\alpha_H)}{2\alpha_F - \alpha_H}. \quad (22)$$

The Sellmeier equations [37] were used to estimate L_α for the PSN-d structures as a function of the fundamental wavelength [Fig. 5(a)]. One observes that the limit imposed by L_α is less restrictive at longer wavelengths. The increase in the optimum length is due to the fact that the reflection coefficients τ_{iq} decrease and the domain length becomes progressively longer as we move to longer wavelengths. With this in mind, we performed an analysis of the second-harmonic conversion efficiency and compared it with a bulk PPLN crystal of length $L = 30$ mm. The crystal for PSN-d structures are $L = L_\alpha$, but limiting at a maximum corresponding to $L = 30$ mm (this occurs at $\lambda > 3$ μm). To calculate the optimum crystal length

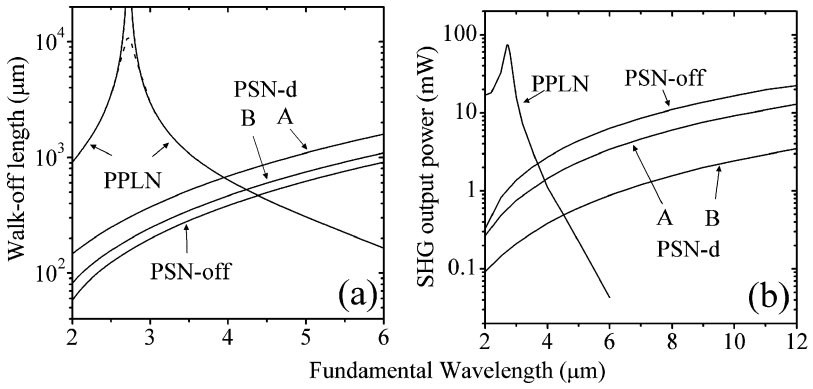

Fig. 6. (a) Walk-off length L_δ for pump pulses of 100 fs in duration in terms of the fundamental wavelength. (b) SHG average output power for crystal lengths $L = L_\delta$ except for PPLN near $\lambda = 2.7$ μm, where crystal lengths were limited by GVD to $L = 10.3$ mm [dashed lines in (a)].

for PSN-off structures, Sellmeier equations for the switch-off domains by ion implantation in GaAs were needed. To the best of our knowledge, these are not available, and, thus, for the purpose of this analysis, two different situations were considered. First, we assumed an ideal situation in which the reflection losses are negligible. As in this case the crystal length is not limited by losses, we chose the same length as in PPLN, $L = 30$ mm. In the second situation, we assumed that the domains in the PSN-off structure have the same refractive index and length as the domains of case B in PSN-d structures. The resulting SHG conversion for 1 W of fundamental pump power is shown in Fig. 5(b). At short wavelengths, the efficiency of the PSN structures is reduced because of the use of shorter crystals (compared to PPLN), which are limited in size by reflection losses [see Fig. 5(a) and (22)]. For $\lambda > 3$ μm, given that all of the crystals were made to have the same length, the efficiency tends to decrease with λ (as the nonlinear terms in (11) and (12) are multiplied by ω and the nonlinear coefficient decreases following Miller's rule). Specifically, in the worst situation for PSN-off devices, where the same losses for PSN-d devices are assumed (solid line), conversion efficiency at long wavelengths can be better than in PPLN, in this example at $\lambda > 2.7$ μm. In the ideal situation in which there are no losses (dashed line), the PSN-off crystal lengths are not limited and, therefore, they could offer better efficiency than PPLN crystals in all of their shared transparency ranges. According to our estimates, waveguide PPLN is always more efficient than PSN-d structures. Only when compared with bulk PPLN, PSN-d can be more efficient at $\lambda > 4$ μm (case A) and $\lambda > 3.7$ μm (case B). This is the situation shown in Fig. 5(b). Finally, this figure also shows that, if the two PSN-d devices are compared at $\lambda < 4.5$ μm, the case B is more efficient (longer crystals are possible), while at $\lambda > 4.5$ μm the case A is the best option (due to the higher FOM).

In the femtosecond-pulse regime, reflection losses are negligible but the optimal crystal length is limited mainly by GVM. To study this limit, we use the walk-off length defined in terms of the pump pulse bandwidth as $L_\delta = 0.4429\lambda^2/(c\delta\Delta\lambda)$ [1]. In Fig. 6(a), we plot L_δ versus the pump wavelength showing the effect of the averaged GVM parameter δ for pulses of 100 fs in duration. One observes that PPLN exhibits a resonant peak near $\lambda = 2.7$ μm where L_δ becomes infinite. At this wavelength, the group velocities for the fundamental and second-harmonic waves are equal and the parameter δ becomes zero. The crystal length is then limited by the GVD [dashed lines in Fig. 6(a)], giving an optimum length of about $L_\delta \approx 10.3$ mm. Fig. 6(a) also shows that, due to the high dispersion present at short wavelengths, the walk-off length L_δ in PSN devices is small. In Fig. 6(b), we plot the SHG average output power for a 100-mW pump. The three structures have lengths that are equal to the walk-off length plot in Fig. 6(a) except for PPLN at wavelengths near $\lambda = 2.7$ μm. In this case, the actual crystal length is the one shown with dashed lines. We observe that, despite the large FOM of PSN-off, the PPLN crystal is more efficient at short wavelengths as it is possible to use a larger crystal for the same bandwidth. However, at longer wavelengths, when the length of the PSN crystals becomes progressively larger than that in PPLN, the PSN structures can be more efficient. In our example, PSN structures are more efficient than PPLN at $\lambda > 3.7$ μm, $\lambda > 3.9$ μm, and $\lambda > 4.5$ μm for the PSN-off, the PSN-d (case A), and PSN-d (case B), respectively.

Finally, it is worth mentioning that, as we move in our analysis from the femtosecond to the CW regime, an intermediate behavior between both regimes is shown. For example, in the picosecond regime, both characteristic lengths L_α and L_δ become important and therefore the crystal length must be chosen accordingly.

IV. Experimental Results

We have implemented, by a regrowth process, a PSN-d waveguide device that corresponds to the best situation of case B, GaAs–$Al_{0.4}Ga_{0.6}As$. The PSN design was restricted to operate at the longest wavelength available with our source $\lambda = 1965$ nm. As discussed in Section III, this is not the most efficient situation, however it proves that the PSN is an operational concept.

The semiconductor structure was fabricated by growing three different layers on a GaAs $\langle 100 \rangle$ substrate. The first layer, $Al_{0.6}Ga_{0.4}As$, was 2 μm thick, followed by a $\sim$0.2-μm layer of $Al_{0.4}Ga_{0.6}As$, and terminated with a 1.15-μm layer of undoped GaAs. The wafer was then processed by etching a 1.1-μm-deep first-order grating with a period of $\Lambda = l_{c1} + l_{c2}$ with $l_{c1} = 2.97$ μm and $l_{c2} = 4.73$ μm [see (19)] into the GaAs

layer. This was followed by the regrowth of two new layers: 2-μm-thick $Al_{0.4}Ga_{0.6}As$ and 0.2-μm-thick $Al_{0.6}Ga_{0.4}As$ over the grating, finishing with a 10-nm GaAs protective cap. Finally, waveguide ridges of 3-, 5-, 8-, and 15-μm widths were etched perpendicular to the grating, and the sample was cleaved into $\sim$1.0- and 0.3-mm-long devices.

To test our PSN devices, we used as a pump source the idler pulses from a synchronously-pumped optical parametric oscillator (OPO) based on a PPLN crystal. As mentioned before, the OPO was tuned to the longest wavelength available to us, 1965 nm. The pulses had a duration of $\Delta\tau < 200$ fs (FWHM) and had an average output power of 20 mW.

These pulses were launched into the waveguides through a $40\times$ aspherical lens that had a numerical aperture of NA $= 0.55$. The output pulses from the device were collected and collimated using a 3-mm-diameter biconvex lens with a focal length of $f = 10$ mm. The SHG and the transmitted fundamental pulses were sent via a stepper motor scanning monochromator for analysis. For measurements of the frequency doubled light a Si photodetector, assisted via lock-in amplification, was used to register the SHG signal at the output slit of the spectrometer. To measure the spectra of the transmitted fundamental light, a Ge filter (antireflection/antireflection coated for 2 μm and with a cut-off wavelength of 1.7 μm) was placed at the entrance at the spectrograph and the Si photodetector was replaced for an InGaSbAs photodiode.

Under these conditions, we tested our samples. We were only able to couple the pump light only through the 15-μm-wide waveguides for both the 1.0- and 0.3-mm-long devices. We believe that the main factor that compromised coupling efficiency on the other narrower core waveguides was not Fresnel losses due to the internal structure of the sample, but the numerical aperture of the waveguide and the guiding conditions. The performance of the 15-μm-wide waveguides for both the 1.0- and 0.3-mm devices was similar. The SHG intensity as a function of the fundamental wavelength power launched into the waveguides is plotted in Fig. 7 (dotted line). In both cases, the data show the expected quadratic response for a QPM-SHG process, as can be seen by the linear fit (solid line in Fig. 7) which has a slope of 1.97. We also verified that the SHG signal vanished when the polarization of the fundamental wavelengths was rotated by 90°.

We then proceeded to explore the bandwidth of our PSN devices. Here it is important to note that the presence of two different materials with different coherence lengths to form one single period makes it difficult to investigate the bandwidth of these crystals. For different pump wavelengths, the change of coherence length for one material is in general different from the change of coherence length of the second material. This translates into an effective reduction in its phase-matching bandwidth. To investigate this point, we decided to explore two different crystal lengths and two close pump wavelengths. Two sets of experiments were performed. In the first one (see Fig. 8, dotted lines), we pumped a 1.1-mm-long PSN crystal with pulses centered at $\lambda = 1950$ nm and having a bandwidth [full-width at half-maximum (FWHM)] of $\Delta\lambda = 36$ nm. Here the pulses were frequency doubled to generate pulses with a bandwidth of $\Delta\lambda = 4.5$ nm [19]. In the second set of measurements (Fig. 8, solid lines), we used a 0.3-mm-long PSN crystal to generate the SHG signal [42], [43]. The OPO was tuned to deliver idler pulses at the central wavelength of $\lambda = 1965$ nm with a bandwidth $\Delta\lambda = 45$ nm. The SHG spectrum measured at the output of these waveguides showed a bandwidth of $\Delta\lambda = 12$ nm. We found that our experimental results disagreed with our calculations by a factor of 35%. Our simulations have shown that this error may be due to a combined effect of having a large GVM together with a constant mismatch in the domain periods, which effectively reduces the crystal size (and the efficiency of the process). Other factors such as waveguiding effects, pulse shape, and frequency chirp might also have some impact.

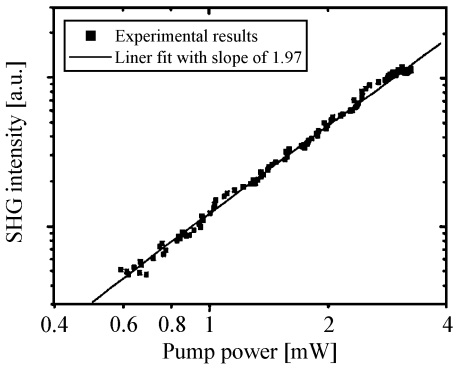

Fig. 7. SHG intensity as a function of fundamental power launched into the waveguide (dotted line) and the best linear fit with slope 1.97 (solid line).

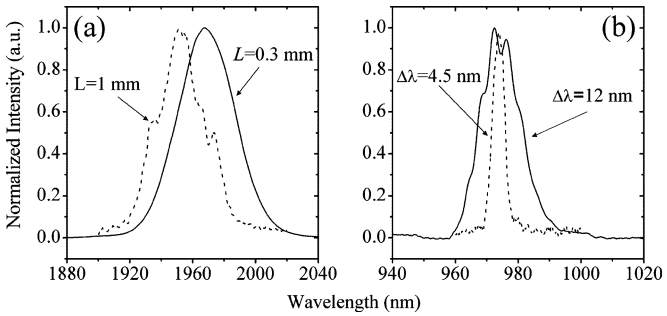

Fig. 8. Spectra of (a) fundamental and (b) SHG pulses for a crystal length $L = 1$ mm (dashed lines) and $L = 0.3$ mm (solid lines).

Finally, the measured conversion efficiency for the average input pump power of $\sim$2 mW was $\sim$0.1%. We attribute such a low efficiency to the fact that the experiment was performed slightly away from the phase-matching condition, with the mismatch due to the inaccuracy in the determination of the domain lengths.

V. Discussion and Conclusion

The present study establishes the theoretical basis for periodically switched nonlinear structures. The developed theory was used to study the special case of a PSN structure based on $Al_xGa_{1-x}As$ due to its high potential applications. The results were then applied in the experimental implementation of such a structure.

The main contribution of the theoretical development presented here is the deduction of the averaged equations describing SHG in a PSN structure. As a result, averaged

parameters, such as GVM, GVD, and, importantly, the effective nonlinear coefficient, were obtained. This allows the use of the well-established theory of parametric interaction applied to PSN. The concept is also applicable to any frequency mixing scheme.

The theoretical analysis of PSN based on $Al_xGa_{1-x}As$ was performed in both CW and femtosecond regimes. The analysis of these structures showed that the main limit in the CW regime was reflection loses, while in the femtosecond regime the efficiency was limited by the large walk-off that is intrinsic in semiconductors. It was shown in both regimes that the PSN-off structure (the nonlinear coefficient is null in alternative domains) was more efficient than PSN-d due to a higher FOM and presumable lower reflection losses. Here, two optimal configurations based on $Al_{0.4}Ga_{0.6}As$–AlAs for case A and $Al_{0.4}Ga_{0.6}As$–GaAs for case B were identified. When compared with bulk PPLN, our numerical analysis has shown that PSN-off devices afford a better solution for SHG in CW. In the femtosecond regime, however, PSN structures offer higher efficiency only at long wavelengths ($\lambda > 4\ \mu$m).

Finally, we have presented preliminary experimental evidence that shows that it is possible to fabricate a QPM structure on GaAs–$Al_xGa_{1-x}As$ waveguides. The data acquired confirm that QPM-SHG occurs inside waveguides when pumped by femtosecond pulses at 1965- and 1950-nm wavelengths. The SHG efficiency of the tested devices was severely limited for two reasons. First, the generated wavelengths were close to the absorption edge of GaAs [23]. Second, at the wavelengths involved in the SHG process, a large GVM was present inside the waveguide. This has a negative impact on the efficiency of the crystal by reducing its phase-matching bandwidth and consequently by also reducing its effective active length.

We therefore conclude that, under optimized conditions, the new QPM method based on a periodically switched nonlinearity can provide a technological advantage when periodically poling cannot be used. The technique is relatively simple and potentially it can be implemented in a broad range of materials.

ACKNOWLEDGMENT

The authors thank Prof. R. Delarue and Dr. D. Yanson for stimulating discussions and helping to prepare samples.

REFERENCES

[1] M. M. Fejer, G. A. Magel, D. H. Jundt, and R. L. Byer, "Quasiphase-matched 2nd harmonic-generation—tuning and tolerances," *IEEE J. Quantum Electron.*, vol. 28, pp. 2631–2654, Nov. 1992.

[2] G. W. Ross, M. Pollnau, P. G. R. Smith, W. A. Clarkson, P. E. Britton, and D. C. Hanna, "Generation of high-power blue light in periodically poled $LiNbO_3$," *Opt. Lett.*, vol. 23, pp. 171–173, 1998.

[3] Y. Chiu, V. Gopalan, M. J. Kawas, T. E. Schlesinger, and D. D. Stancil, "Integrated optical device with second-harmonic generator, electrooptic lens, and electrooptic scanner in $LiTaO_3$," *J. Lightwave Technol.*, vol. 17, pp. 462–465, Mar. 1999.

[4] M. Pierrou, F. Laurell, H. Karlsson, T. Kellner, C. Czeranowsky, and G. Huber, "Generation of 740 mW of blue light by intracavity frequency doubling with a first-order quasiphase-matched $KTiOPO_4$ crystal," *Opt. Lett.*, vol. 24, pp. 205–207, 1999.

[5] L. E. Myers, R. C. Eckardt, M. M. Fejer, R. L. Byer, W. R. Bosenberg, and J. W. Pierce, "Quasiphase-matched optical parametric oscillators in bulk periodically-poled $LiNbO_3$," *J. Opt. Soc. Amer. B*, vol. 12, pp. 2102–2116, 1995.

[6] I. Shoji, T. Kondo, and R. Ito, "Second-order nonlinear susceptibilities of various dielectric and semiconductor materials," *Opt. Quantum Electron.*, vol. 34, pp. 797–833, 2002.

[7] E. Lallier, M. Brevignon, and J. Lehoux, "Efficient second-harmonic generation of a CO_2 laser with a quasiphase-matched GaAs crystal," *Opt. Lett.*, vol. 23, pp. 1511–1513, 1998.

[8] D. Zheng, L. A. Gordon, Y. S. Wu, R. S. Feigelson, M. M. Fejer, R. L. Byer, and K. L. Vodopyanov, "16-μm infrared generation by difference-frequency mixing in diffusion-bonded-stacked GaAs," *Opt. Lett.*, vol. 23, pp. 1010–1012, 1998.

[9] T. Skauli, K. L. Vodopyanov, T. J. Pinguet, A. Schober, O. Levi, L. A. Eyres, M. M. Fejer, J. S. Harris, B. Gerard, L. Becouarn, E. Lallier, and G. Arisholm, "Measurement of the nonlinear coefficient of orientation-patterned GaAs and demonstration of highly efficient second- harmonic generation," *Opt. Lett.*, vol. 27, pp. 628–630, 2002.

[10] O. Levi, T. J. Pinguet, T. Skauli, L. A. Eyres, K. R. Parameswaran, J. S. Harris, M. M. Fejer, T. J. Kulp, S. E. Bisson, B. Gerard, E. Lallier, and L. Becouarn, "Difference frequency generation of 8-mu m radiation in orientation-patterned GaAs," *Opt. Lett.*, vol. 27, pp. 2091–2093, 2002.

[11] L. A. Eyres, P. J. Tourreau, T. J. Pinguet, C. B. Ebert, J. S. Harris, M. M. Fejer, L. Becouarn, B. Gerard, and E. Lallier, "All-epitaxial fabrication of thick, orientation-patterned GaAs films for nonlinear optical frequency conversion," *Appl. Phys. Lett.*, vol. 79, pp. 904–906, 2001.

[12] M. W. Street, N. D. Whitbread, C. J. Hamilton, B. Vogele, C. R. Stanley, D. C. Hutchings, J. H. Marsh, J. S. Aitchison, G. T. Kennedy, and W. Sibbett, "Modification of the second-order optical nonlinearities in AlGaAs asymmetric multiple quantum well waveguides by quantum well intermixing," *Appl. Phys. Lett.*, vol. 70, pp. 2804–2806, 1997.

[13] K. Moutzouris, S. V. Rao, M. Ebrahimzadeh, A. De Rossi, V. Berger, M. Calligaro, and V. Ortiz, "Efficient second-harmonic generation in birefringently phase- matched GaAs/Al_2O_3 waveguides," *Opt. Lett.*, vol. 26, pp. 1785–1787, 2001.

[14] A. S. Helmy, D. C. Hutchings, T. C. Kleckner, J. H. Marsh, A. C. Bryce, J. M. Arnold, C. R. Stanley, J. S. Aitchison, C. T. A. Brown, K. Moutzouris, and M. Ebrahimzadeh, "Quasi phase matching in GaAs-AlAs superlattice waveguides through bandgap tuning by use of quantum-well intermixing," *Opt. Lett.*, vol. 25, pp. 1370–1372, 2000.

[15] S. J. B. Yoo, M. M. Fejer, R. L. Byer, and J. S. Harris, "2nd-order susceptibility in asymmetric quantum-wells and its control by proton-bombardment," *Appl. Phys. Lett.*, vol. 58, pp. 1724–1726, 1991.

[16] J. P. Bouchard, M. Tetu, S. Janz, D. X. Xu, Z. R. Wasilewski, P. Piva, U. G. Akano, and I. V. Mitchell, "Quasiphase matched second-harmonic generation in an $Al_xGa_{1-x}As$ asymmetric quantum-well waveguide using ion-implantation- enhanced intermixing," *Appl. Phys. Lett.*, vol. 77, pp. 4247–4249, 2000.

[17] S. J. B. Yoo, R. Bhat, C. Caneau, and M. A. Koza, "Quasiphase-matched 2nd-harmonic generation in AlGaAs wave-guides with periodic domain inversion achieved by wafer-bonding," *Appl. Phys. Lett.*, vol. 66, pp. 3410–3412, 1995.

[18] S. J. B. Yoo, C. Caneau, R. Bhat, M. A. Koza, A. Rajhel, and N. Antoniades, "Wavelength conversion by difference frequency generation in AlGaAs waveguides with periodic domain inversion achieved by wafer bonding," *Appl. Phys. Lett.*, vol. 68, pp. 2609–2611, 1996.

[19] E. U. Rafailov, P. Loza-Alvarez, C. T. A. Brown, W. Sibbett, R. M. De La Rue, P. Millar, D. A. Yanson, J. S. Roberts, and P. A. Houston, "Second-harmonic generation from a first-order quasiphase- matched GaAs/AlGaAs waveguide crystal," *Opt. Lett.*, vol. 26, pp. 1984–1986, 2001.

[20] T. K. S. Koh, Y. Shiraki, and R. Ito, "CFA5," presented at the Conf. Lasers and Electrooptics-Europe, Nice, France, Sept. 10–15, 2000.

[21] C. B. Ebert, L. A. Eyres, M. M. Fejer, and J. S. Harris, "MBE growth of antiphase GaAs films using GaAs/Ge/GaAs heteroepitaxy," *J. Cryst. Growth*, vol. 202, pp. 187–193, 1999.

[22] S. Koh, T. Kondo, M. Ebihara, T. Ishiwada, H. Sawada, H. Ichinose, I. Shoji, and R. Ito, "GaAs/Ge/GaAs sublattice reversal epitaxy on GaAs (100) and (111) substrates for nonlinear optical devices," *Jpn. J. Appl. Phys. Part 2—Lett.*, vol. 38, pp. L508–L511, 1999.

[23] F. A. Katsriku, B. M. A. Rahman, and K. T. V. Grattan, "Finite-element analysis of second-harmonic generation in AlGaAs waveguides," *IEEE J. Quantum Electron.*, vol. 36, pp. 282–289, Feb. 2000.

[24] D. C. Hutchings and T. C. Kleckner, "Quasi phase matching in semiconductor waveguides by intermixing: optimization considerations," *J. Opt. Soc. Amer. B*, vol. 19, pp. 890–894, 2002.

[25] H. Komine, W. H. Long, J. W. Tully, and E. A. Stappaerts, "Quasiphase-matched second-harmonic generation by use of a total-internal-reflection phase shift in gallium arsenide and zinc selenide plates," *Opt. Lett.*, vol. 23, pp. 661–663, 1998.

[26] A. Chowdhury, H. M. Ng, M. Bhardwaj, and N. G. Weimann, "Second-harmonic generation in periodically poled GaN," *Appl. Phys. Lett.*, vol. 83, pp. 1077–1079, 2003.

[27] P. J. Chandler, L. Zhang, and P. D. Townsend, "Double wave-guide in $LiNbO_3$ by ion-implantation," *Appl. Phys. Lett.*, vol. 55, pp. 1710–1712, 1989.

[28] S. Janz, M. Buchanan, F. Chatenoud, J. P. McCaffrey, R. Normandin, U. G. Akano, and I. V. Mitchell, "Modification of the 2nd-order optical susceptibility in Alxga1-Xas by ion-beam-induced amorphization," *Appl. Phys. Lett.*, vol. 65, pp. 216–218, 1994.

[29] M. Kuhnelt, T. Leichtner, S. Kaiser, B. Hahn, H. P. Wagner, D. Eisert, G. Bacher, and A. Forchel, "Quasiphase matched second harmonic generation in ZnSe waveguide structures modulated by focused ion beam implantation," *Appl. Phys. Lett.*, vol. 73, pp. 584–586, 1998.

[30] O. P. Kowalski, C. J. Hamilton, S. D. McDougall, J. H. Marsh, A. C. Bryce, R. M. De la Rue, B. Vogele, C. R. Stanley, C. C. Button, and J. S. Roberts, "A universal damage induced technique for quantum well intermixing," *Appl. Phys. Lett.*, vol. 72, pp. 581–583, 1998.

[31] S. D. McDougall, O. P. Kowalski, C. J. Hamilton, F. Camacho, B. C. Qiu, M. L. Ke, R. M. De La Rue, A. C. Bryce, and J. H. Marsh, "Monolithic integration via a universal damage enhanced quantum- well intermixing technique," *IEEE J. Select. Topics Quantum Electron.*, vol. 4, pp. 636–646, July/Aug. 1998.

[32] M. Ohashi, T. Kondo, R. Ito, S. Fukatsu, Y. Shiraki, K. Kumata, and S. S. Kano, "Determination of quadratic nonlinear-optical coefficient of $Al_xGa_{1-X}As$ system by the method of reflected 2nd harmonics," *J. Appl. Phys.*, vol. 74, pp. 596–601, 1993.

[33] S. Janz, C. Fernando, H. Dai, F. Chatenoud, M. Dion, and R. Normandin, "Quasiphase-matched 2nd-harmonic generation in reflection from $Al_xGa_{1-X}As$ heterostructures," *Opt. Lett.*, vol. 18, pp. 589–591, 1993.

[34] P. D. Townsend, P. J. Chandler, and L. Zhang, *Optical Effects of Ion Implantation*. Cambridge, U.K.: Cambridge Univ. Press, 1994.

[35] D. J. L. Birkin, E. U. Rafailov, W. Sibbett, L. Zhang, Y. Liu, and I. Bennion, "Near-transform-limited picosecond pulses from a gain-switched InGaAs diode laser with fiber Bragg gratings," *Appl. Phys. Lett.*, vol. 79, pp. 151–152, 2001.

[36] P. Loza-Alvarez, M. Ebrahimzadeh, W. Sibbett, D. T. Reid, D. Artigas, and M. Missey, "Femtosecond second-harmonic pulse compression in aperiodically poled lithium niobate: a systematic comparison of experiment and theory," *J. Opt. Soc. Amer. B*, vol. 18, pp. 1212–1217, 2001.

[37] R. J. Deri and M. A. Emanuel, "Consistent formula for the refractive-index of $Al_xGa_{1-X}As$ below the band-edge," *J. Appl. Phys.*, vol. 77, pp. 4667–4672, 1995.

[38] C. B. Clausen, O. Bang, and Y. S. Kivshar, "Spatial solitons and induced Kerr effects in quasiphase-matched quadratic media," *Phys. Rev. Lett.*, vol. 78, pp. 4749–4752, 1997.

[39] J. F. Corney and O. Bang, "Solitons in quadratic nonlinear photonic crystals," *Phys. Rev. E*, vol. 6404, p. art. no.-047601, 2001.

[40] ——, "Modulational instability in periodic quadratic nonlinear materials," *Phys. Rev. Lett.*, vol. 8713, p. art. no.-133901, 2001.

[41] D. H. Jundt, "Temperature-dependent Sellmeier equation for the index of refraction, n(e), in congruent lithium niobate," *Opt. Lett.*, vol. 22, pp. 1553–1555, 1997.

[42] E. U. Rafailov, P. Loza-Alvarez, D. Artigas, and W. Sibbett, "Efficient frequency conversion from a novel QPM semiconductor waveguide crystal," in *Proc. 13th Int. Conf. Ultrafast Phenom.*, Vancouver, BC, Canada, 2002, pp. 167–169.

[43] E. U. Rafailov, P. Loza-Alvarez, D. Artigas, C. T. A. Brown, R. M. d. l. Rue, and W. Sibbett, "Novel first-order quasiphase matched semiconductor waveguide crystal for frequency conversion," in *Proc. CLEO*, Long Beach, CA, 2002, paper CWL5.

David Artigas received the B.Sc. degree in physics from the Universitat de Barcelona, Barcelona, Spain, in 1990 and the Ph.D. degree from the Universitat Politècnica de Catalunya (UPC), Barcelona, Spain, in 1995.

He subsequently became a Senior Researcher at UPC. Since 1998, he has held the position of Lecturer in electromagnetic fields and photonics at the Telecommunication School, UPC. In 2001, he stayed for one year at the Heriot-Watt University, Edinburgh, U.K., as a Research Visitor. His main research interests include theoretical analysis and modeling in nonlinear optics, ultrafast fenomena, optical parametric processes, and quasi-phase-matching engineering.

Edik U. Rafailov (M'00) received the M.Sc. degree (with honors) in physics from the Samarkand State University, Samarkand, U.S.S.R., in 1986, and the Ph.D. degree in the physics of semiconductors and dielectrics from A.F.Ioffe Institute, St. Petersburg, Russia, in 1991.

He stayed on as a Senior Researcher at the Institute until 1997 when he joined the University of St. Andrews, St. Andrews, U.K., as a Research Fellow. His main research interests include novel high-power continuous-wave, short, ultrashort-pulse, and high-frequency laser diodes, integrated and nonlinear optics, compact diode-based visible/infrared lasers, and laser diode applications. He has coauthored over 85 journal and conference papers on these topics.

Pablo Loza-Alvarez received the B.Sc. degree in physics from the Universidad Nacional Autónoma de México (UNAM), México DF, México, in 1992, the M.Sc. degree in physics from the Centro de Investigación científica y de Estudios Superiores de Ensenada (CICESE), Ensenada, México, in 1995, and the Ph.D. degree in laser physics from the University of St. Andrews, St. Andrews, U.K., in 2000.

He stayed with the University of St. Andrews for two years in a postdoctoral posotion. In 2002, he moved to the Institut de Cienciès Fotòniques, Universidad Politécnica de Cataluña (UPC-ICFO), Barcelona, Spain, where he currently holds a tenure track position. His main research interests include nonlinear microscopy, nonlinear optics, and ultrashort-pulse lasers. He has coauthored over 44 journal and conference papers on these topics.

Wilson Sibbett received the B.Sc. degree in physics and the Ph.D. degree from Queen's University, Belfast, Ireland, in 1970 and 1973, respectively.

He carried out graduate research studies for his Ph.D. degree in laser physics at Queen's University and later at the Blackett Laboratory of Imperial College, London, U.K., where he subsequently became a Lecturer and Reader in physics. In 1985, he joined the University of St. Andrews, St. Andrews, U.K., as a Professor of Natural Philosophy and Head of the Department of Physics and where, since 1994, he has been the Director of Research. His main research interests include ultrashort-pulse lasers, diode lasers and diode-pumped solid-state lasers, nonlinear/waveguide optics, and applications in photomedicine and has coauthored over 280 journal publications on these topics.

Prof. Sibbett is a Fellow of the Royal Society (London), the Royal Society of Edinburgh, the Institute of Physics, and the Optical Society of America.